

# Formation of Binary Black Holes Similar to GW190521 with a Total Mass of $\sim 150 M_{\odot}$ from Population III Binary Star Evolution

Tomoya Kinugawa<sup>(1)\*</sup>, Takashi Nakamura<sup>(2)</sup>, and Hiroyuki Nakano<sup>(3)</sup>

<sup>1</sup>*Institute for Cosmic Ray Research, The University of Tokyo, Kashiwa, Chiba 277-8582, Japan*

<sup>2</sup>*Department of Physics, Graduate School of Science, Kyoto University, Kyoto 606-8502, Japan*

<sup>3</sup>*Faculty of Law, Ryukoku University, Kyoto 612-8577, Japan*

3 December 2020

## ABSTRACT

In the case of zero-metal (population III or Pop III) stars, we show that the total mass of binary black holes from binary Pop III star evolution can be  $\sim 150 M_{\odot}$ , which agrees with the mass of the binary black hole GW190521 recently discovered by LIGO/Virgo. The event rate of such binary black hole mergers is estimated as  $0.13\text{--}0.66 (\rho_{\text{SFR}}/(6 \times 10^5 M_{\odot}/\text{Mpc}^3)) \text{Err}_{\text{sys}} \text{yr}^{-1} \text{Gpc}^{-3}$ , where  $\rho_{\text{SFR}}$  and  $\text{Err}_{\text{sys}}$  are the cumulative comoving mass density of Pop III stars depending on star formation rate and the systematic errors depending on uncertainties in the Pop III binary parameters, respectively. The event rate in our fiducial model with  $\rho_{\text{SFR}} = 6 \times 10^5 M_{\odot}/\text{Mpc}^3$  and  $\text{Err}_{\text{sys}} = 1$  is  $0.13\text{--}0.66 \text{yr}^{-1} \text{Gpc}^{-3}$ , which is consistent with the observed value of  $0.02\text{--}0.43 \text{yr}^{-1} \text{Gpc}^{-3}$ .

**Key words:** stars: population III, binaries: general relativity, gravitational waves, black hole mergers

## 1 INTRODUCTION

GW190521, observed in the LIGO/Virgo third observing run (O3a) (Abbott et al. 2020a,b), is a gravitational-wave (GW) signal from a merging binary black hole (BH) with a primary BH mass of  $71\text{--}106 M_{\odot}$ <sup>1</sup>, and a secondary BH mass of  $48\text{--}83 M_{\odot}$ . The remnant BH after the merger has a mass of  $126\text{--}170 M_{\odot}$ , and thus this object can be considered as an intermediate-mass BH in the mass range  $100\text{--}1000 M_{\odot}$ . The redshift of GW190521 is  $0.48\text{--}1.1$ , while the merger rate density is estimated as  $0.02\text{--}0.43 \text{yr}^{-1} \text{Gpc}^{-3}$ .

Here, we should note that the two component masses of GW190521 are possibly within the pair-instability supernova (PISN) mass gap for metallicity  $Z \geq 0.001 Z_{\odot}$ . In Woosley (2017), this PISN mass gap is described as “No black holes between  $52$  and  $133 M_{\odot}$  are expected from stellar evolution in close binaries”. In more detail, Leung et al. (2019) discussed pulsational PISNe (PPISNe) for  $Z \geq 0.001 Z_{\odot}$  by simulating a helium core without the hydrogen envelope, as simulation of the whole star is computationally expensive. They obtained a lower bound of the PISN

mass gap of approximately  $50 M_{\odot}$ , indicating that merging of two BHs with mass  $\lesssim 50 M_{\odot}$  is needed to form a BH with a mass  $\gtrsim 50 M_{\odot}$  (e.g., Fragione et al. 2020b).

However, the upper limit of the mass of BHs for population (Pop) III stars with  $Z = 0$  is different from that for  $Z \geq 0.001 Z_{\odot}$ . Because Pop III stars do not tend to lose the envelope, they will have a different lower bound of the PISN mass gap to that of Pop II stars. The CO core mass ( $M_{\text{CO}}$ ) range of PPISNe is approximately  $40\text{--}60 M_{\odot}$  (Heger & Woosley 2002; Heger et al. 2003; Umeda & Nomoto 2008; Waldman 2008; Yoshida et al. 2016). Calculations of Pop III star evolution (Marigo et al. 2001; Heger & Woosley 2002; Heger et al. 2003; Ekström et al. 2008; Tanikawa et al. 2019) show that to form such a massive CO core, the zero-age main sequence (ZAMS) mass of Pop III stars has to exceed  $\sim 100 M_{\odot}$ . Furthermore, Yoon et al. (2012) and Chatzopoulos & Wheeler (2012) computed the evolution of Pop III metal-free ( $Z = 0$ ) massive stars, and Table 1 in Chatzopoulos & Wheeler (2012) shows that a nonrotating Pop III star with a ZAMS mass of  $M_{\text{ZAMS}} = 75 M_{\odot}$  becomes a BH in the core collapse. Thus, the formation of BHs with  $M \lesssim 80 M_{\odot}$  from Pop III stars is a possible natural explanation of the existence of GW190521-like binary BHs for binary Pop III stars (see Figure 12 in Yoon et al. (2012) and Figure 5 in Chatzopoulos & Wheeler (2012)).

\* E-mail: kinugawa@icrr.u-tokyo.ac.jp

<sup>1</sup> Here, all values estimated by LIGO/Virgo are shown using the symmetric 90% credible interval.

We should note that many proposals and discussions to explain BHs within the PISN mass gap and their dynamics were made immediately after the announcement of GW190521: primordial BHs (Carr et al. 2019; De Luca et al. 2020; Vovchenko et al. 2020), numerical relativity simulations on extremely eccentric (head-on) mergers (Calderón Bustillo et al. 2020a), numerical relativity simulations on a high-eccentricity, precessing model (Gayathri et al. 2020), GW data analysis using an eccentric waveform model (Romero-Shaw et al. 2020), possible existence beyond the Standard Model explanations (Sakstein et al. 2020), an analysis of BH mass functions based on the ten binary BHs observed in GWTC-1 (Wang et al. 2020), BH masses in a modified gravitational theory (Moffat 2020), repeated BH mergers in star clusters (Fragione et al. 2020a), head-on collisions of two horizonless vector boson stars (Calderón Bustillo et al. 2020b), and binary BHs straddling the PISN mass gap (Fishbach & Holz 2020). Of the above references, De Luca et al. (2020) estimated the event rate of GW190521-like binary BHs as  $\approx 1.1 \text{ yr}^{-1}$  for  $(M_1, M_2 > 65M_\odot)$  and  $\approx 0.8 \text{ yr}^{-1}$  for  $(M_1 > 85M_\odot, M_2 > 65M_\odot)$  in a primordial BH scenario, assuming the detectability threshold (signal-to-noise ratio (SNR) = 8) for the O3 sensitivity. Here,  $M_1$  and  $M_2$  are the masses of the primary and secondary objects, respectively.

On the other hand, the existence of mass-gap BHs like GW190521 has been suggested by Pop III binary star evolution (Kinugawa et al. 2016; Kinugawa et al. 2020b; Tanikawa et al. 2020), which is supported by a recent calculation of Pop III stellar evolution (Farrell et al. 2020). However, the event rate has not yet been discussed, including the various models shown in the previous paragraph, except for a primordial BH model by De Luca et al. (2020). In this Letter, we discuss the formation process of GW190521-like binary BHs from Pop III stars and estimate the event rate from population synthesis simulations of Pop III binary stars.

## 2 ANALYSIS

First, we discuss the effect of the rotational velocity of Pop III stars at ZAMS. When the end state of a Pop III star is described by a Kerr BH, the angular momentum of the BH should satisfy the following inequality:

$$J_{\text{BH}} < M \frac{GM}{c}. \quad (1)$$

Assuming no angular momentum loss of the star up to the formation of BH, we may regard the angular momentum at ZAMS as equal to that of the final BH, that is,  $J_{\text{ZAMS}} = J_{\text{BH}}$ . The Pop III star at ZAMS has the rotational energy

$$\begin{aligned} E_{\text{rot}} &\sim \frac{J_{\text{ZAMS}}^2}{I} \\ &= \frac{J_{\text{BH}}^2}{I}, \end{aligned} \quad (2)$$

where  $I$  is the moment of inertia of the Pop III star. The gravitational energy of the star is written as

$$E_{\text{grav}} \sim \frac{GM^2}{R}, \quad (3)$$

where  $R$  is the stellar radius. By comparing the rotational energy (Eq. (2)) with the gravitational energy (Eq. (3)) and

using Eq. (1), we have

$$\begin{aligned} \frac{E_{\text{rot}}}{E_{\text{grav}}} &< \frac{GM^2 R}{Ic^2} \\ &= \frac{GM}{c^2 R \kappa}, \end{aligned} \quad (4)$$

where  $\kappa$  is defined by  $I = \kappa MR^2$ . Using the values of  $M$ ,  $R$ , and  $\kappa$  for Pop III stars at ZAMS, we can estimate the upper limit of the effect of rotation. The stellar radius at ZAMS ( $R_{\text{ZAMS}}$ ) is given by Kinugawa et al. (2014) as

$$\begin{aligned} \frac{R_{\text{ZAMS}}}{R_\odot} &= 1.22095 + 2.70041 \times 10^{-2} \left( \frac{M}{10 M_\odot} \right) \\ &\quad + 0.135427 \left( \frac{M}{10 M_\odot} \right)^2 \\ &\quad - 1.95541 \times 10^{-2} \left( \frac{M}{10 M_\odot} \right)^3 \\ &\quad + 8.7585 \times 10^{-4} \left( \frac{M}{10 M_\odot} \right)^4. \end{aligned} \quad (5)$$

Using Eq. (5), for  $M_{\text{ZAMS}} = 10\text{--}100 M_\odot$  we have

$$\frac{GM}{c^2 R} \sim 1.6 \times 10^{-5} - 5 \times 10^{-5}. \quad (6)$$

From Eqs. (6) and (4), if  $\kappa \gg 5 \times 10^{-5}$ , we may ignore the effect of rotation. Thus, we can use the results of the evolution of spherically symmetric Pop III stars. In practice,  $\kappa = 0.21$  for the core, and  $O(0.1)\text{--}O(0.01)$  for the outer layer (Hurley et al. 2002; Kinugawa et al. 2014); hence, the rotational energy is at most 0.01 times the gravitational energy<sup>2</sup>. Therefore, we can use the results of the evolution of spherically symmetric Pop III stars as a good approximation to rotating ones.

Next, we discuss the evolution of Pop III binaries. In our previous work (Kinugawa et al. 2020b), we simulated the evolution of Pop III binaries using population synthesis simulations for various models with different initial conditions: initial mass function, initial mass ratio, separation and eccentricity distributions of binaries, binary evolution parameters such as mass transfer rate of the donor, fraction of transferred stellar mass in the accretion process, common envelope parameters, and tidal coefficient factor. As a result, we found that the chirp mass<sup>3</sup> distribution of binary BHs formed from Pop III star binaries has a peak at  $M_{\text{chirp}} \sim 30 M_\odot$  and the merger rate density of the Pop III binary BHs at  $z = 0$  is in the range  $3.34\text{--}21.2 \text{ yr}^{-1} \text{ Gpc}^{-3}$  for seven different models. This is consistent with the LIGO/Virgo result of  $9.7\text{--}101 \text{ yr}^{-1} \text{ Gpc}^{-3}$  (Abbott et al. 2019).

In Kinugawa et al. (2020b), we considered only the PISNe without the remnant if the CO core mass is more than  $60 M_\odot$ , corresponding to the initial total mass  $M_{\text{initial}}$  of  $\sim 130 M_\odot$  (Heger & Woosley 2002). In this Letter, we also consider the PISNe when the CO core mass is between  $40 M_\odot$  and  $60 M_\odot$  (e.g., Yoshida et al. 2016).

<sup>2</sup> For polytropes, we have  $\kappa = 0.4, 0.261, 0.155, 0.0754, 0.0226,$  and  $0.00690$  for the polytropic indexes of  $n = 0, 1, 2, 3, 4,$  and  $4.5$ , respectively.

<sup>3</sup> Here, the chirp mass is defined by

$$M_{\text{chirp}} = \frac{(M_1 M_2)^{3/5}}{(M_1 + M_2)^{1/5}}. \quad (7)$$

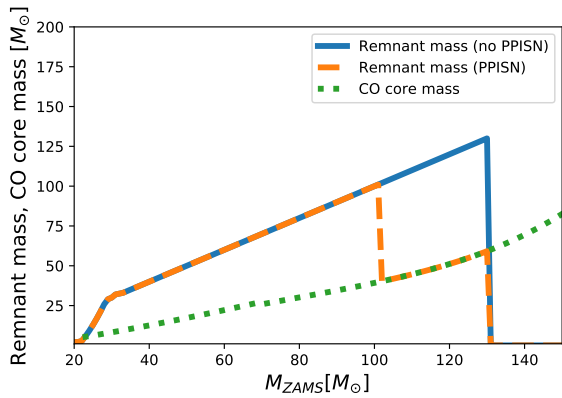


**Figure 1.** Remnant mass and CO core mass as a function of the zero-age main-sequence mass of the progenitor star. The blue solid line shows the model without mass ejection at PPISN (no PPISN), and the orange dashed line shows the model with mass ejection (PPISN). The green dotted line is the CO core mass.

In previous studies on the mass ejection of PPISNe (e.g. Yoshida et al. 2016; Leung et al. 2019), only Pop II stars that had already lost the hydrogen-rich envelope before PPISN were considered. In contrast, Pop III PPISN progenitors tend to keep the hydrogen envelope due to the lack of metals, and thus the envelope mass may be halted. In this circumstance, we consider two possible extreme models and consider the reality to be between these two extremes. One is the model without mass ejection at PPISN (no (mass ejection) PPISN model). This model is the same as the fiducial model of Kinugawa et al. (2020b). In the other extreme case, the hydrogen and helium envelopes are totally ejected by PPISN, and the remnant mass is equal to the CO core mass (PPISN model). We have two extreme estimations of the event rate of GW190521-like binary BH mergers from the above two extreme models: the no-mass ejection model gives the upper bound of the event rate, whereas the PPISN model gives the lower bound.

Figure 1 shows the remnant mass and CO core mass as a function of the ZAMS mass of the progenitor star. In this figure, the blue solid and orange dashed lines show the models without mass ejection at PPISN (no PPISN) and with mass ejection (PPISN), respectively. The CO core mass is shown by the green dotted line. Although binaries can lose the envelope via the binary interaction, a single Pop III star can evolve up to  $\sim 100 M_{\odot}$  BH even in the worst case, which corresponds to the orange dashed line in Figure 1.

The distribution functions of the initial conditions for evolution of Pop III binaries for our models are summarized in Table 1<sup>4</sup>. The functional forms are shown for the initial mass function ( $M_1$ ), distribution of initial mass ratio ( $q = M_1/M_2$ ), distribution of orbital separation ( $a$ ), and eccentricity ( $e$ ) distributions of binaries with the range of the parameter. For the star formation rate of Pop III stars, we use the same redshift dependence as that of de Souza et al. (2011), but a value a factor of three smaller for the constraint of the Pop III star formation rate (Inayoshi et al. 2016), which is compatible with the cosmological Thomson scat-

<sup>4</sup> See Kinugawa et al. (2020b) for details of the binary evolution.

tering optical depth of the cosmic microwave background (CMB) measured by Planck Collaboration et al. (2016). To estimate the event rate of GW190521-like binaries, we use  $10^6$  Pop III binaries for each model and pick up binary BHs with chirp masses that exceed  $56 M_{\odot}$ , because the chirp mass of GW190521 is estimated as  $56\text{--}77 M_{\odot}$  (Abbott et al. 2020a).

Figures 2 and 3 show the mass distribution of primary and secondary BHs with chirp masses that exceed  $56 M_{\odot}$  and merge within the Hubble time. If we consider perfect envelope loss due to PPISN, the maximum BH mass is  $\sim 80 M_{\odot}$  from the orange lines in Figures 2 and 3. Some Pop III stars with ZAMS masses of  $\sim 90\text{--}100 M_{\odot}$ , which avoid the PPISN and lose part of the envelope via mass transfer, can be the progenitors of such massive BHs. On the other hand, if there is no envelope loss by Pop III PPISN, the maximum mass reaches  $\sim 105 M_{\odot}$  from the blue lines in Figures 2 and 3. Note that the grey areas in Figures 2 and 3 are the mass ranges of the primary and secondary BHs of GW190521, respectively. Thus, our two extreme theoretical predictions shown by the blue and orange lines are both consistent with the observed mass values of the primary and secondary BHs.

Here, let us define  $\rho_{\text{SFR}}$  and  $Err_{\text{sys}}$  by the cumulative comoving mass density of Pop III stars depending on the star formation rate, and the systematic error depending on uncertainties in the Pop III binary parameters. We first consider the case with  $\rho_{\text{SFR}} = (6 \times 10^5 M_{\odot}/\text{Mpc}^3)$  and  $Err_{\text{sys}} = 1$ . In the no-mass ejection model, the current event rate of GW190521-like binary BH mergers is estimated as  $0.66 \text{ yr}^{-1} \text{ Gpc}^{-3}$ . In contrast, the perfect PPISN model gives  $0.13 \text{ yr}^{-1} \text{ Gpc}^{-3}$ . Given that these two values originate from the extreme theoretical models, our fiducial model is defined as a model between the two extreme models with a rate from  $0.13$  to  $0.66 \text{ yr}^{-1} \text{ Gpc}^{-3}$ . The event rate of the general model can be expressed as  $0.13\text{--}0.66 (\rho_{\text{SFR}}/(6 \times 10^5 M_{\odot}/\text{Mpc}^3)) Err_{\text{sys}} \text{ yr}^{-1} \text{ Gpc}^{-3}$ .  $\rho_{\text{SFR}} = 6 \times 10^5 M_{\odot}/\text{Mpc}^3$  corresponds to the cumulative mass density of Pop III stars calculated by Inayoshi et al. (2016), assuming a flat IMF. Kinugawa et al. (2016) checked the dependence of  $Err_{\text{sys}}$  on binary parameters such as the IMF, common envelope parameter, mass loss fraction of the mass transfer, and BH natal kick. They obtained the worst model in which the worst combination of parameters is used. In the worst model,  $Err_{\text{sys}} \sim 0.05$ , while  $Err_{\text{sys}} \sim 3.4$  in the best model. Using these estimates, we find that the event rate is in the range  $0.0065\text{--}2.24 (\rho_{\text{SFR}}/(6 \times 10^5 M_{\odot}/\text{Mpc}^3)) \text{ yr}^{-1} \text{ Gpc}^{-3}$ . Except for near the worst model or the smallest-mass-density model, the theoretical rate is consistent with the observed range of  $0.02\text{--}0.43 \text{ yr}^{-1} \text{ Gpc}^{-3}$  from GW190521.

Finally, we estimate the maximum observable redshift  $z_{\text{max}}$  for the LIGO O3a-Livingston (O3a-L), LIGO O5, Einstein Telescope (ET-B), and Cosmic Explorer (CE2). Using the inspiral–merger–ringdown waveform shown in Nakamura et al. (2016), we calculate the SNR of GW events in fitted sensitivity curves for the O3a-L ( $f_{\text{low}} = 10 \text{ Hz}$ ), O5 ( $f_{\text{low}} = 10 \text{ Hz}$ ), ET-B ( $f_{\text{low}} = 1 \text{ Hz}$ ), and CE2 ( $f_{\text{low}} = 5 \text{ Hz}$ ) used in Kinugawa et al. (2020a). Here,  $f_{\text{low}}$  is the lower frequency cutoff and we set the higher frequency cutoff at  $f_{\text{high}} = 3000 \text{ Hz}$ , although we do not need such a high frequency for the heavy binary BHs considered below. Subsequently, the maximum observable redshift by setting the

**Table 1.** Distribution functions of initial conditions in evolution of Pop III binaries. Functional forms are shown for the initial mass function ( $M_1$ ), distribution of initial mass ratio ( $q$ ), distribution of orbital separation ( $a$ ), and eccentricity ( $e$ ) distributions of binaries with the range of the parameter.  $M_1$  denotes the primary mass and  $q = M_1/M_2$  is the mass ratio, where  $M_2$  denotes the secondary mass.

Initial mass function	Initial mass ratio	Initial separation	Initial eccentricity
flat	flat	logflat	Power law (index:1)
$10M_\odot < M_1 < 150M_\odot$	$10M_\odot/M_1 < q < 1$	$\log a_{\min} < \log(a/R_\odot) < 6$	$0 < e < 1$

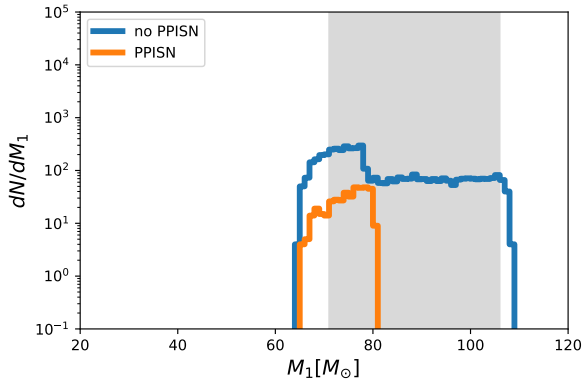


**Figure 2.** Primary BH mass distribution for binary BHs with chirp mass of  $\geq 56 M_\odot$  that merge within the Hubble time. The blue line shows the model without mass ejection at PPISN (no PPISN), and the orange line shows the model with mass ejection (PPISN). The grey area is the mass range of the primary BH of GW190521.

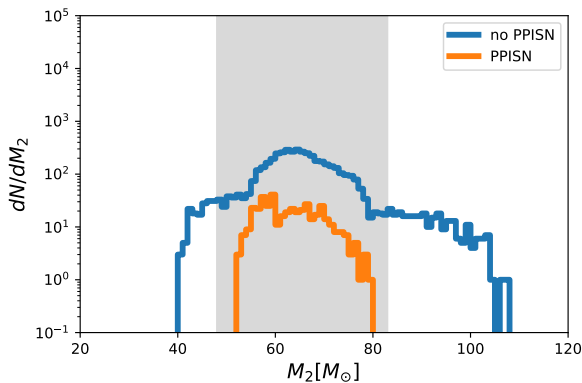


**Figure 3.** Same as Figure 2, but for the secondary BH mass distribution and the mass range of the secondary BH of GW190521.

averaged SNR = 8 is obtained for a binary BH with masses ( $75 M_\odot$ ,  $75 M_\odot$ ) as 0.709 for O3a-L, 1.60 for O5, 10.8 for ET-B, and 19.3 for CE2. For a binary BH with masses ( $80 M_\odot$ ,  $80 M_\odot$ ),  $z_{\max}$  becomes 0.734 for O3a-L, 1.61 for O5, 10.6 for ET-B, and 18.4 for CE2. The above calculations are summarized in Table 2.

### 3 DISCUSSION

In the population synthesis simulations of Pop III binary stars, we can simultaneously explain the formation of bi-

**Table 2.** Maximum observable redshift  $z_{\max}$  for GW190521-like binary BHs for four ground-based GW detector configurations: LIGO O3a-Livingston (O3a-L), LIGO O5 (O5), Einstein Telescope (ET-B), and Cosmic Explorer (CE2). The mass is shown in solar masses  $M_\odot$ .

$(M_1, M_2)$	O3a-L	O5	ET-B	CE2
(75, 75)	0.709	1.60	10.8	19.3
(80, 80)	0.734	1.61	10.6	18.4

aries that consist of a BH and mass-gap compact object (MGCO) with a mass of  $2\text{--}5 M_\odot$  (Kinugawa et al. 2020a) like GW190814, and those that consist of BHs with masses of  $\sim 80 M_\odot$  within the PISN mass gap for Pop III stars like GW190521. The first detected GW event, GW150914, the BH masses of which are  $\sim 30 M_\odot$ , had been predicted before its first detection by Kinugawa et al. (2014). It is of great interest that our Pop III model can interpret the origins of three different classes of GW sources, that is, massive binary BHs with masses of  $\sim 30 M_\odot$  like GW150914, BH and MGCO binaries with masses of  $\sim 2.5 M_\odot$  like GW190814, and very massive binary BHs with masses of  $\sim 80 M_\odot$  like GW190521. It will be triple the fun! If the origin of massive binary BHs is Pop III field binaries, the merger rate density has a peak at  $z \sim 10$  (Kinugawa et al. 2020a). Thus, the future work of GW observatories such as ET (Hild et al. 2011), CE (Reitze et al. 2019), and DECIGO (Seto et al. 2001) can verify whether our model is correct or not.

The Pop III binary BH merger rate strongly depends on the Pop III star formation rate (SFR) and IMF, which are still observationally uncertain because no Pop III star has ever been observed. In the case of the Pop III SFR, there is a constraint on the density of gas from the Thomson scattering optical depth obtained from CMB observation (Visbal et al. 2015; Inayoshi et al. 2016). On the other hand, the merger rate also depends on the Pop III IMF. In our previous study (Kinugawa et al. 2016), we verified the IMF dependence of Pop III binary BHs using the flat, logflat, and Salpeter IMFs. The number of merging massive binary BHs ( $M_{\text{total}} \sim 150 M_\odot$ ) for the logflat IMF decreases to a value about two thirds that of the flat IMF. Although we have no observational data of Pop III stars, some numerical simulations and semi-analytical calculations have been performed to estimate the Pop III IMF. Hirano et al. (2014) and Susa et al. (2014) showed the Pop III stellar formation in star-forming minihalos using cosmological simulations, and obtained the Pop III IMF for  $\sim 10\text{--}1000 M_\odot$ . Recent simulations (Hirano & Bromm 2017; Susa 2019) suggest that fragmentation causes the typical mass of Pop III stars to be

small, although there are still some uncertainties such as the merging of fragments and the magnetic effect.

On the other hand, [Tarumi et al. \(2020\)](#) have estimated the Pop III IMF from the metallicity distribution analysis of the inhomogeneous metal mixing effect calibrated by the metallicity distribution function of extremely metal-poor (EMP) stars. They showed that the Pop III IMF is proportional to  $M^{-0.5}$  ( $2-180M_{\odot}$ ), which is different from the flat IMF adopted in this study. To compare the effect of different IMFs, in this study we employ a simple method using the probability, although population synthesis calculations are needed for detailed analysis. As shown in the footnote, the probability of having GW190521-like binary BHs for the Tarumi IMF is approximately 78% of that for our flat IMF<sup>5</sup>. However, this is a simple order-of-magnitude argument and more population synthesis simulations are needed for a wider class of possible IMFs. Theoretically, when we consider different IMFs, it is not clear which macroscopic quantity is fixed: the total number of stars, the total mass, or the total luminosity. This problem should also be solved in the future. The future work of GW observatories such as ET, CE, and DECIGO can detect massive binary BH mergers at  $z \gtrsim 10$ . The comparison between the binary BH mass distribution at high redshift and theoretical estimations of the Pop III IMF might reveal the Pop III stellar mass distribution.

[Liu & Bromm \(2020\)](#) have recently considered another possibility of Pop III binary BH mergers originating from dynamical capture. They calculated the merger rate of Pop III binary BHs made by dynamical capture in cosmological hydrodynamic simulations. Although their merger rate ( $0.04 \text{ yr}^{-1} \text{ Gpc}^{-3}$ ) is smaller than that for our field binary case, the Pop III binary BHs formed by dynamical capture might have different features from Pop III binary BHs made by field binaries, such as large eccentricity by dynamical friction and larger typical mass of BHs, because of the absence of mass loss in binary interactions. These differences might be observed by ET or other future GW observations. The origin of binary BHs will be made clear by the GW observation of the redshift  $z > 10$  (see Table 2), i.e., in the ET-B era. This is because the cumulative event rate of Pop I/II binary BHs saturates at  $z < 5$ , and that of Pop III binary BHs saturates at  $z \sim 10$  ([Nakamura et al. 2016](#)).

In this paper, we did not focus on the spin values of binary BHs. The spin estimation for GW190521 has a large uncertainty as the nondimensional spin parameters  $\chi_1 = 0.07-0.96$  and  $\chi_2 = 0.09-0.97$ , although there is a weak preference

<sup>5</sup> Let us choose the minimum and maximum masses of Pop III stars as  $M_{\min} = 10M_{\odot}$  and  $M_{\max} = 150M_{\odot}$ , respectively. We also define IMFs for our case and the Tarumi case as  $f_{\text{flat}}(M) = C_{\text{flat}} = \text{constant}$  and  $f_{\text{Tarumi}}(M) = C_{\text{Tarumi}}/M^{0.5}$ , respectively. By fixing the total number of stars ( $N_{\text{tot}}$ ), we have  $C_{\text{flat}} = N_{\text{tot}}/(M_{\max} - M_{\min})$  and  $C_{\text{Tarumi}} = N_{\text{tot}}/[2\{(M_{\max})^{0.5} - (M_{\min})^{0.5}\}]$ . The probability of a star with a mass  $M$  in the interval  $dM$  is proportional to  $f(M)dM$ , where  $f(M)$  is an IMF. Therefore, the relative probability ( $p(M)$ ) of a star of mass  $M$  that exists in the Tarumi IMF compared with the flat IMF is given by  $p(M) = f_{\text{Tarumi}}(M)/f_{\text{flat}}(M)$ . Using  $p(M)$ , the relative probability of the existence of a binary with masses  $M_1$  and  $M_2$  is equal to  $p_b(M_1, M_2) = p(M_1)p(M_2)$  if there is no correlation. For GW190521,  $M_1 \sim 88M_{\odot}$  and  $M_2 \sim 65M_{\odot}$ , and thus we obtain  $p_b(M_1, M_2) \sim 0.78$ .

for a spinning, precessing binary BH, i.e., the BH spins may be misaligned from the orbital angular momentum. Furthermore, according to [LIGO Scientific Collaboration and Virgo Collaboration, \(2020\)](#), the orientation of spins projected on the orbital plane is not determined. By observing the long inspiral phase with space-based GW detectors (see, e.g., B-DECIGO in [Isoyama et al. \(2018\)](#) and TianQin in [Mei et al. \(2020\)](#)), we will be able to access more precise information on the spins. Whether Pop III stars rotate or not is related to the abundance patterns of EMP stars ([Takahashi et al. 2014](#); [Choplin et al. 2019](#)). If we can obtain more precise information on the spins from the future work of space-based GW detectors, it might be possible to impose a constraint on the Pop III stellar rotation, and to consider the rotation effect on the abundance patterns of EMP stars.

## ACKNOWLEDGMENT

We would like to greatly thank the anonymous referee for their useful comments to improve our paper. We thank Ataru Tanikawa and Takahiro S. Yamamoto for useful discussions on the mass-gap BH and the BH spins of GW190521. T. K. acknowledges support from the University of Tokyo Young Excellent Researcher program. T. N. acknowledges support from JSPS KAKENHI Grant No. JP15H02087. H. N. acknowledges support from JSPS KAKENHI Grant Nos. JP16K05347 and JP17H06358. We thank Editage (www.editage.com) for English language editing.

## DATA AVAILABILITY

Results will be shared on reasonable request to corresponding author.

## REFERENCES

- Abbott B., et al., 2019, *Phys. Rev. X*, 9, 031040  
 Abbott R., et al., 2020a, *Phys. Rev. Lett.*, 125, 101102  
 Abbott R., et al., 2020b, *ApJ*, 900, L13  
 Calderón Bustillo J., Sanchis-Gual N., Torres-Forné A., Font J. A., 2020a, arXiv e-prints, p. [arXiv:2009.01066](#)  
 Calderón Bustillo J., et al., 2020b, arXiv e-prints, p. [arXiv:2009.05376](#)  
 Carr B., Clesse S., Garcia-Bellido J., Kuhnel F., 2019, arXiv e-prints, p. [arXiv:1906.08217](#)  
 Chatzopoulos E., Wheeler J., 2012, *ApJ*, 748, 42  
 Choplin A., Tominaga N., Ishigaki M. N., 2019, *A&A*, 632, A62  
 De Luca V., Desjacques V., Franciolini G., Pani P., Riotto A., 2020, arXiv e-prints, p. [arXiv:2009.01728](#)  
 Ekström S., Meynet G., Chiappini C., Hirschi R., Maeder A., 2008, *A&A*, 489, 685  
 Farrell E. J., Groh J. H., Hirschi R., Murphy L., Kaiser E., Ekström S., Georgy C., Meynet G., 2020, arXiv e-prints, p. [arXiv:2009.06585](#)  
 Fishbach M., Holz D. E., 2020, arXiv e-prints, p. [arXiv:2009.05472](#)  
 Fragione G., Loeb A., Rasio F. A., 2020a, arXiv e-prints, p. [arXiv:2009.05065](#)  
 Fragione G., Loeb A., Rasio F. A., 2020b, *ApJL*, 895, L15  
 Gayathri V., et al., 2020, arXiv e-prints, p. [arXiv:2009.05461](#)  
 Heger A., Woosley S. E., 2002, *ApJ*, 567, 532

- Heger A., Fryer C. L., Woosley S. E., Langer N., Hartmann D. H., 2003, *ApJ*, **591**, 288
- Hild S., et al., 2011, *Classical and Quantum Gravity*, **28**, 094013
- Hirano S., Bromm V., 2017, *MNRAS*, **470**, 898
- Hirano S., Hosokawa T., Yoshida N., Umeda H., Omukai K., Chiaki G., Yorke H. W., 2014, *ApJ*, **781**, 60
- Hurley J. R., Tout C. A., Pols O. R., 2002, *MNRAS*, **329**, 897
- Inayoshi K., Kashiyama K., Visbal E., Haiman Z., 2016, *MNRAS*, **461**, 2722
- Isoyama S., Nakano H., Nakamura T., 2018, *PTEP*, 2018, 073E01
- Kinugawa T., Inayoshi K., Hotokezaka K., Nakauchi D., Nakamura T., 2014, *MNRAS*, **442**, 2963
- Kinugawa T., Miyamoto A., Kanda N., Nakamura T., 2016, *MNRAS*, **456**, 1093
- Kinugawa T., Nakamura T., Nakano H., 2020a, arXiv e-prints, p. [arXiv:2007.13343](https://arxiv.org/abs/2007.13343)
- Kinugawa T., Nakamura T., Nakano H., 2020b, *MNRAS*, **498**, 3946
- LIGO Scientific Collaboration and Virgo Collaboration, 2020, <https://dcc.ligo.org/P2000158/public>
- Leung S.-C., Nomoto K., Blinnikov S., 2019, *ApJ*, **887**, 72
- Liu B., Bromm V., 2020, *MNRAS*, **497**, 2839
- Marigo P., Girardi L., Chiosi C., Wood P. R., 2001, *A&A*, **371**, 152
- Mei J., et al., 2020, arXiv e-prints, p. [arXiv:2008.10332](https://arxiv.org/abs/2008.10332)
- Moffat J. W., 2020, arXiv e-prints, p. [arXiv:2009.04360](https://arxiv.org/abs/2009.04360)
- Nakamura T., et al., 2016, *PTEP*, 2016, 093E01
- Planck Collaboration et al., 2016, *A&A*, **596**, A108
- Reitze D., et al., 2019, *Bull. Am. Astron. Soc.*, **51**, 035
- Romero-Shaw I. M., Lasky P. D., Thrane E., Calderon Bustillo J., 2020, arXiv e-prints, p. [arXiv:2009.04771](https://arxiv.org/abs/2009.04771)
- Sakstein J., Croon D., McDermott S. D., Straight M. C., Baxter E. J., 2020, arXiv e-prints, p. [arXiv:2009.01213](https://arxiv.org/abs/2009.01213)
- Seto N., Kawamura S., Nakamura T., 2001, *Phys. Rev. Lett.*, **87**, 221103
- Susa H., 2019, *ApJ*, **877**, 99
- Susa H., Hasegawa K., Tominaga N., 2014, *ApJ*, **792**, 32
- Takahashi K., Umeda H., Yoshida T., 2014, *ApJ*, **794**, 40
- Tanikawa A., Yoshida T., Kinugawa T., Takahashi K., Umeda H., 2019, arXiv e-prints, p. [arXiv:1906.06641](https://arxiv.org/abs/1906.06641)
- Tanikawa A., Susa H., Yoshida T., Trani A. A., Kinugawa T., 2020, arXiv e-prints, p. [arXiv:2008.01890](https://arxiv.org/abs/2008.01890)
- Tarumi Y., Hartwig T., Magg M., 2020, *ApJ*, **897**, 58
- Umeda H., Nomoto K., 2008, *ApJ*, **673**, 1014
- Visbal E., Haiman Z., Bryan G. L., 2015, *MNRAS*, **453**, 4456
- Vovchenko V., Brandt B. B., Cuteri F., Endrődi G., Hajkarim F., Schaffner-Bielich J., 2020, arXiv e-prints, p. [arXiv:2009.02309](https://arxiv.org/abs/2009.02309)
- Waldman R., 2008, *ApJ*, **685**, 1103
- Wang Y.-Z., Tang S.-P., Liang Y.-F., Han M.-Z., Li X., Jin Z.-P., Fan Y.-Z., Wei D.-M., 2020, arXiv e-prints, p. [arXiv:2009.03854](https://arxiv.org/abs/2009.03854)
- Woosley S., 2017, *ApJ*, **836**, 244
- Yoon S., Dierks A., Langer N., 2012, *A&A*, **542**, A113
- Yoshida T., Umeda H., Maeda K., Ishii T., 2016, *MNRAS*, **457**, 351
- de Souza R. S., Yoshida N., Ioka K., 2011, *A&A*, **533**, A32